International Journal of Pharmaceutics 692 (2026) 126649

Contents lists available at ScienceDirect

International Journal of Pharmaceutics

journal homepage: www.elsevier.com/locate/ijpharm

ANN-assisted UV imaging for non-destructive dissolution prediction of HPMC matrix tablets

Orsolya Péterfi [a], Lilla Alexandra Mészáros [a,*], Bence Szabó-Szőcs [a], Máté Ficzere [a], Brigitta Nagy [a], Emese Sipos [b], Sándor Lenk [c], Zsombor Kristóf Nagy [a], Dorián László Galata [d,**]

[a] Department of Organic Chemistry and Technology, Faculty of Chemical Technology and Biotechnology, Budapest University of Technology and Economics, Műegyetem Rkp. 3., H-1111 Budapest, Hungary
[b] Department of Pharmaceutical Industry and Management, Faculty of Pharmacy, George Emil Palade University of Medicine, Pharmacy, Sciences and Technology of Targu Mures, Gheorghe Marinescu Street 38, 540142 Targu Mures, Romania
[c] Department of Atomic Physics, Institute of Physics, Budapest University of Technology and Economics, Műegyetem Rkp 3., H-1111 Budapest, Hungary
[d] School of Engineering, University of Leicester, University Rd, Leicester LE1 7RH, United Kingdom

ARTICLE INFO

Keywords:
Dissolution prediction
Artificial neural network
Machine vision
UV imaging
PAT
Extended release

ABSTRACT

This study investigates the use of UV imaging combined with artificial neural networks (ANNs) to estimate the dissolution behaviour of extended-release hydroxypropyl methylcellulose (HPMC) matrix tablets. UV illumination enables the detection of HPMC, allowing polymer-specific optical information to be extracted. Caffeine was used as the model active pharmaceutical ingredient, and HPMC served as the matrix-forming polymer. Formulations were prepared with HPMC contents ranging from 5% to 35%. The ANN models were trained using colourimetric information extracted from UV images of the tablets. Among all models evaluated, the one based on the blue channel of the RGB colour space showed the best performance, achieving an average f_2 similarity factor of 80.68 on the dissolution curves of the external validation set. To evaluate the performance of the trained model on an external test set under dynamic conditions, powder blends with different HPMC contents were introduced sequentially, resulting in gradual changes in tablet composition. The trained model reflected these formulation changes in the predicted dissolution profiles, capturing the shifts in release behaviour associated with the varying HPMC levels throughout the experiment. UV imaging provided relevant input for dissolution modelling and enabled the rapid, non-destructive assessment of formulation-dependent drug release. The results therefore extend the applicability of imaging-based methods to excipient-level formulation changes.

1. Introduction

Dissolution testing provides direct information on the release characteristics of oral solid dosage forms under standardized conditions. The procedure is indispensable in formulation development and quality assurance, where it is employed to evaluate product performance, support regulatory compliance, and identify variability arising from composition or process parameters (Azarmi et al., 2007). Drug release behaviour is sensitive to numerous factors, including particle size (Chu et al., 2012), solid-state properties (Baghel et al., 2018), salt form (Bharate, 2021), content uniformity, and manufacturing conditions (Kale et al., 2009; Loh et al., 2015; Markl et al., 2021), as well as the concentration and grade of matrix-forming polymers such as hydroxypropyl methylcellulose (HPMC), which play a critical role in controlling gel-layer formation and release kinetics in extended-release systems (Guiastrennec et al., 2017). Even minor deviations in these parameters can lead to tablets that fail to meet established dissolution criteria. If such outliers remain undetected, they may compromise therapeutic efficacy or patient safety.

Although widely used in quality control, conventional dissolution testing is destructive, time-consuming, restricted to limited sampling, meaning that only a fraction of the batch can be analysed (Hernandez et al., 2016; Pawar et al., 2016). These limitations have encouraged efforts toward alternative, non-destructive strategies for assessing drug

* Corresponding author.
** Corresponding author.
E-mail addresses: meszaros.lilla.alexandra@vbk.bme.hu (L.A. Mészáros), dlg22@leicester.ac.uk (D.L. Galata).

https://doi.org/10.1016/j.ijpharm.2026.126649
Received 8 December 2025; Received in revised form 26 January 2026; Accepted 31 January 2026
Available online 5 February 2026

release. However, monitoring the concentration of polymeric matrix formers such as HPMC during production remains challenging. Their spectral appearance in near-infrared are typically broad and strongly overlapping with those of other excipients (Galata et al., 2023).

The introduction of Process Analytical Technology (PAT) and Quality by Design (QbD) frameworks has driven the development of surrogate approaches capable of predicting dissolution behaviour using in-line measurements (Beg et al., 2019). PAT tools including near-infrared (NIR) (Zhong et al., 2022), Raman (Karimi-Jafari et al., 2021), ultraviolet–visible (UV–VIS) (Brands et al., 2023), terahertz pulse (Bawuah et al., 2021), light-induced fluorescence (Sørensen et al., 2022), and optical coherence tomography (Fink et al., 2024; Sacher et al., 2024) sensors to monitor critical quality attributes such as tablet disintegration time (Mészáros et al., 2024a), tensile strength (Lee et al., 2021), active pharmaceutical ingredient (API) content (Chavez et al., 2015), and moisture levels (Peters et al., 2017), which are critical for understanding and controlling manufacturing processes.

Data obtained from PAT sensors have also been applied to predict the dissolution behaviour of pharmaceutical products, with data-driven techniques such as partial least squares (PLS) regression commonly used to develop surrogate dissolution models. PLS extracts latent variables from multivariate datasets to capture linear relationships between dissolution profiles and diverse inputs such as spectral measurements, formulation attributes and process parameters (Hernandez et al., 2016; Yekpe et al., 2015; Zeng et al., 2022; Zhao et al., 2019). Mechanistic models provide a complementary strategy based on physicochemical principles and offer greater interpretability, although their substantial computational requirements often limit real-time applicability. (Ferdoush and Gonzalez, 2024; Kalný et al., 2021; Matsunami et al., 2025).

Artificial neural networks (ANNs) have also been adopted for dissolution prediction, offering a means to capture complex, non-linear relationships between material attributes, process parameters, and release profiles (Ibrić et al., 2012). Previous ANN-based studies relied primarily on variables such as particle size, composition or compression force as model inputs (Galata et al., 2021, 2019; Lourenço et al., 2025; Madzarevic et al., 2019). These have been reported to outperform linear approaches such as PLS and multiple linear regression (MLR), while in some cases achieving predictive performance comparable to mechanistic models (Horkovics-Kovats et al., 2022; Lourenço et al., 2025; Nagy et al., 2019). Comparative studies have examined the performance of ANN, PLS, support vector machine (SVM), and ensemble regression tree (ERT) models for predicting dissolution profiles. ANN models predict dissolution profiles using a single model across all time points, whereas SVM and ERT approaches rely on independently predicted values at each time point. As a result, SVM and ERT predictions could, in some cases, exhibit non-monotonic behavior between consecutive dissolution values, which is inconsistent with the cumulative nature of dissolution profiles (Galata et al., 2021). In comparison with PLS-based dissolution models, ANN approaches have also been reported to achieve lower prediction errors. In particular, Nagy et al. showed that ANN models outperformed PLS when predicting dissolution from multivariate inputs, attributing this to the linear nature of PLS models, which limits their ability to represent non-linear relationships between the inputs and the dissolution response (Nagy et al., 2019).

Nevertheless, ANN-based approaches depend strongly on the availability of high-quality training data and often remain product-specific, which can limit their broader applicability.

Data derived from NIR and Raman spectra have been utilized for predicting the dissolution profiles of various dosage forms, including extended-release and immediate-release tablets, as well as pellets (Nagy et al., 2019; Péterfi et al., 2025, 2023; Wu et al., 2024). Zeng et al. utilized Raman mapping combined with PLS regression modeling to predict the dissolution profiles of sustained-release tablets formulated with varying HPMC content (Zeng et al., 2023). Li et al. demonstrated that NIR spectra could be coupled with both partial least squares regression (PLSR) and ANN to predict the dissolution profiles of sinomenine sustained-release tablets formulated with HPMC (Li et al., 2023). Convolutional neural networks (CNNs) have also been utilized to predict dissolution profiles based on Raman and NIR chemical maps, which offer detailed spatial information about formulations containing matrix-forming polymers (Galata et al., 2023).

Alongside spectroscopic methods, increasing attention has been directed toward machine vision that combines image acquisition with multivariate data analysis to offer a cost-efficient and real-time quality assessment. Visible (VIS) imaging has been applied mainly to detect process-induced variations; for example, changes in compression force produced distinct differences in surface morphology, and consequently dissolution behaviour. However, VIS imaging-based methods rely on surface texture and colour information, and therefore provide limited sensitivity to formulation-driven differences, particularly in the case of visually uniform formulations, such as white tablets (Mészáros et al., 2024a).

Ultraviolet (UV) and multispectral imaging has emerged as a versatile tool for characterizing solid dosage forms, offering both spatial and spectral information. Applications include the visualization of component distributions (Wu et al., 2014), the assessment of coating thickness (Novikova et al., 2017), the surface analysis of pellet-based systems (Novikova et al., 2016), and the evaluation of tablet hardness and API content (Klukkert et al., 2016). Previous studies have investigated the feasibility of UV imaging for in-line analysis of tablet API content. Brands et al. implemented an in-line multispectral UV/VIS approach for monitoring the content uniformity of theophylline tablets (Brands et al., 2023), while Ficzere et al. demonstrated the feasibility of UV-based analysis of pimobendane tablets using single-wavelength measurements (Ficzere et al., 2025). Mészáros et al. used UV/VIS imaging to predict dissolution behaviour indirectly through API content variations and surface texture variations caused by compression force (Mészáros et al., 2024b), further illustrating that imaging can capture optical changes related to API content and process parameters. However, imaging-based methods had not yet been applied to detect excipient-related formulation differences.

The aim of this work is to develop a machine vision-based method for predicting the dissolution profiles of extended-release tablets. In contrast to previous UV/VIS imaging approaches, which primarily relied on the well-established UV responsiveness of active pharmaceutical ingredients or surface texture-related features to predict dissolution behaviour, the present work directly targets excipient-level formulation differences. Given that dissolution is a critical quality attribute and HPMC concentration has a strong impact on gel formation and drug release, capturing these formulation-level differences is particularly important. Unlike APIs, excipients such as HPMC do not exhibit an obvious or widely exploited UV response, making their imaging-based characterization considerably less straightforward and far less explored. UV imaging was combined with ANNs to detect excipient-related differences in multi-excipient formulations, using either full colour histograms or features obtained through principal component analysis. A key objective is to show that based on information gathered from the images acquired with a commercially available camera and $UV_{\sim 270nm}$ illumination applicable to detect changes in HPMC concentration and predict the corresponding effects on the dissolution behavior of extended-release tablets. To further explore its application, the approach is evaluated during tableting in continuous mode, where different powder blends are introduced sequentially into the press, leading to gradual changes in tablet composition, providing a means to test whether the system can capture variability in the dissolution profile as it arises. The study examines the feasibility of UV imaging-based non-destructive input for ANN-based dissolution prediction and its potential role for in-process quality monitoring.

2. Materials and methods

2.1. Materials

In this study, extended-release tablets were prepared which contained anhydrous caffeine (BASF, Ludwigshafen, Germany) as model active pharmaceutical ingredient. Hydroxypropyl methylcellulose (HPMC) 2208 (Methocel^{TM}, K4M, Colourcon Ltd., Kent, UK) with a viscosity of 4000 mPas and 19–24 w/w% methoxyl and 7–12 w/w% hydroxypropyl substitution was used as hydrophilic matrix, dibasic calcium phosphate (Anhydrous Emcompress, JRS Pharma GmbH, Rosenberg, Germany) as filler and magnesium stearate (MgSt) (Faci S.P. A., Carasco, Italy) as lubricant.

2.2. Sample preparation

A total of ten formulations were prepared by varying the HPMC content between 5% and 35% (Table 1). The changes in the HPMC content allowed the evaluation of the polymer specific effect on the dissolution profile. The amount of dibasic calcium phosphate was adjusted according to the HPMC concentrations, while the quantities of all other excipients remained constant. Specifically, the concentrations of anhydrous caffeine and MgSt were set at 10% and 1%, respectively.

The model API and dibasic calcium phosphate were initially blended using a multifunctional continuous twin-screw blender (TS16, Quick 2000 Ltd, Hungary), operating at 100 rpm, to ensure a homogeneous API distribution. This step was critical to prevent the formation of large caffeine agglomerates in the samples. Subsequently, HPMC was mixed using a QUICKmill Lab multifunctional mixing apparatus (Quick 2000 Ltd., Tiszavasvári, Hungary) for 5 min. Finally, 1% MgSt was added to the mixing vessel, and the mixture was further homogenized for 1 min. Each formulation was prepared with a batch size of 50 g.

The powder blends were compressed using a Dott Bonapace CPR-6 (Dott Bonapace, Italy) eccentric tablet press, equipped with an 8 mm diameter flat-faced single punch and utilizing a compression force of 12 ± 1 kN. The target tablet weight was 100 ± 4 mg. 10 tablets were prepared for each formulation. Seven formulations were assigned to the sample set for model generation, while three intermediate compositions (7.5%, 20%, and 32.5% HPMC) served as the external validation set. The tablets for these 10 formulations were obtained individually by using the tablet press in non-continuous mode. In this case, the required amount of material was weighed for each tablet and placed into the die before compression.

In order to present an application example of the obtained model, another sample set was produced (external test set). The samples of the external test set were obtained with the tablet press operated in continuous mode using a feeder shoe to introduce dynamic composition change. Initially, 20 g of material from the formulation containing 20% HPMC was placed into the gravity feeder. As the powder level decreased (approximately after 150 tablets), the mixture containing 32.5% HPMC was added subsequently, followed by a final mixture containing 7.5% HPMC. A total of 500 tablets were obtained this way while the press operated in continuous mode. In this experiment, our aim was to demonstrate the capability of the UV imaging method to detect compositional shifts during the tableting process. By introducing the next mixture after the previous powder was nearly depleted, this resulted in a short transition phase between the two formulations. Analysis of the UV images was also used to gain insight into the dynamics of the compositional shift.

Table 1
Powder blend composition for the training, external validation, and external test sets.

Batch	Anhydrous caffeine (w/w%)	HPMC (w/w %)	$CaHPO_4$ (w/w %)	MgSt (w/w %)
Powder blend composition – Sample set for the model generation				
1	10	5	84	1
2	10	10	79	1
3	10	15	74	1
4	10	20	69	1
5	10	25	64	1
6	10	30	59	1
7	10	35	54	1
Powder blend composition – External validation samples				
1	10	7.5	81.5	1
2	10	20	69	1
3	10	32.5	56.5	1
Powder blend composition – External test samples				
1	10	20	69	1
2	10	32.5	56.5	1
3	10	7.5	81.5	1

2.3. Fluorescent spectroscopy

A tablet consisting solely of HPMC was analysed by fluorescence spectroscopy to characterize the intrinsic fluorescence of the matrix-forming polymer. Fluorescence spectroscopy measurements were performed using an RF-6000 spectrofluorometer (Shimadzu Corporation, Kyoto, Japan) equipped with a solid-sample holder. The excitation wavelength was set to 270 nm, with slit bandwidths of 5 nm for both excitation and emission, and a scan speed of 200 nm min^{-1}. An IHU310 long-pass filter (Isuzu Glass, Osaka, Japan) was used to block scattered excitation light during measurements in the 300–600 nm range. For measurements in the 600–700 nm range, an R60 long-pass filter (Hoya, Tokyo, Japan) was employed to suppress both scattered excitation light and second-order diffraction arising from fluorescence emitted between 300 and 350 nm.

2.4. Image acquisition

The images of the tablets were captured using an in-house developed, automated system. The imaging system consisted of a Canon 650D (Canon, Tokyo, Japan) digital single-lens reflex (DSLR) camera, which was equipped with a Canon EFS 18–55 mm objective (Canon, Tokyo, Japan) mounted via a reversing ring. The illumination was provided with a custom-made ring light, containing light-emitting diodes (LED) operating at ~ 270 nm. Images were captured with a resolution of 5184 by 3456 pixels, while the exposure time was set to 3.2 s. All measurements were performed inside a black box to prevent ambient light interference. Fig. 1 presents the setup of the developed UV imaging system. The system enabled computer-controlled automatic movement of the camera along the X, Y, and Z axes, allowing precise positioning above the samples. Tablets were placed in a custom-designed holder, ensuring consistent spacing and alignment throughout image acquisition. Images were taken from both sides of each tablet.

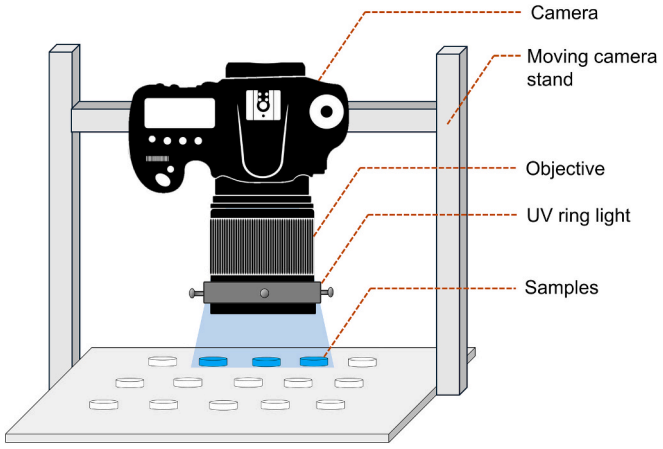

Fig. 1. Measurement setup of the automatic UV imaging system.

2.5. In vitro dissolution testing

Dissolution testing of the tablets was performed using a Pharmatest PTWS 600 dissolution tester (Pharma Test Apparatebau AG, Hainburg, Germany) with the paddle method (apparatus 2). The dissolution medium consisted of 900 mL of distilled water, maintained at a constant temperature of 37 ± 0.5°C, and stirred at 50 rpm. The concentration of dissolved caffeine was monitored over a 5-hour period at 19 sampling time points (2.5, 5, 7.5, 10, 15, 20, 30, 45, 60, 75, 90, 105, 120 min, followed by sampling every 30 min up to 300 min) using an on-line coupled Agilent 8453 UV–Vis spectrophotometer (Hewlett-Packard, Palo Alto, USA). Absorbance was measured at 272 nm using 10 mm cuvettes, based on a preliminary calibration. The peak at 272 nm corresponding to a π-π* electronic transition was chosen because the other caffeine-related peak with notably stronger absorbance at 205 nm is more sensitive to interference, and its absorbance in the utilized concentration range was too strong to be reliably measured. A 100% dissolution value was defined as the target concentration of 10% w/w. In the case of the sample set for model generation, 10 tablets were dissolved for each composition, corresponding to 70 tablets in total. For the 3 external validation compositions, 3 tablets were analysed for each composition (nine tablets in total). Out of the 500 tablets manufactured for the external test set in continuous tableting mode, 12 tablets were selected for dissolution measurement.

2.6. Data analysis

2.6.1. Image analysis

Image processing was carried out using an algorithm developed in MATLAB 2022a (MathWorks, Natick, MA, USA). In this case, the workflow focused on extracting colourimetric information from the images (See Fig. 2). The analysis began with the application of the circle detection based on Hough Transform (CHT) to isolate the tablet region from the background. Once the tablet area was identified, RGB histograms were extracted to quantify the distribution of red, green, and blue pixel intensities within each tablet region. Subsequently, the images were converted into the CIELAB colour space and histograms were then obtained for each of the L* (lightness), a* (green–red), and b* (blue–yellow) components. In the RGB colour space, each component (R, G, B) ranges from 0 to 255. In the CIELAB colour space, L* ranges from 0 to 100, while a* and b* range from − 127 to + 127. For each tablet, data from the two sides were averaged.

2.6.2. Dissolution prediction models

Dissolution prediction models were developed in MATLAB 2022a (MathWorks, Natick, MA, USA) using the Neural Network Toolbox 8.3. PLS Toolbox 7.8.2. (Eigenvector Research, USA) for used for data preprocessing. As the initial step, the histogram data were preprocessed through normalization and mean centering. For most models, principal component analysis (PCA) was then applied to the histograms, and the first five principal components (PCs) were extracted for each tablet. The number of PCs was chosen as a compromise between information retention and dimensionality reduction, providing compact descriptors. These PC scores served as input data for the feedforward, fully connected ANN models. Two models were developed for the B value, one using principal components and the other using selected ranges of the original histogram values without applying principal component analysis. For the model generation sample set the resulting data were subsequently split at random into subsets for model training, validation, and internal testing in a 70–15–15% ratio.

All network architectures comprised an input layer, a single hidden layer, and an output layer with 19 neurons corresponding to the dissolution time points. The hidden layer used a hyperbolic tangent sigmoid activation function, while a linear function was applied in the output layer.

Bayesian regularization backpropagation algorithm was used for training. This algorithm optimizes a loss function that combines the sum of squared errors with a penalty on the magnitude of the network weights, thereby explicitly balancing data fitting with model complexity. If a weight does not reduce the prediction error, this weight value is decreased during the optimization step, so weights, with limited influence on the model output, converge toward small values. Bayesian regularization is particularly suitable for relatively small datasets, as it limits overfitting and decreases sensitivity to the data partitioning and initialisation conditions. The Bayesian regularization approach automatically adjusts the effective number of parameters in the network by modifying the regularization parameters during training. This results in a more robust model that generalizes better to unseen data, as it prevents

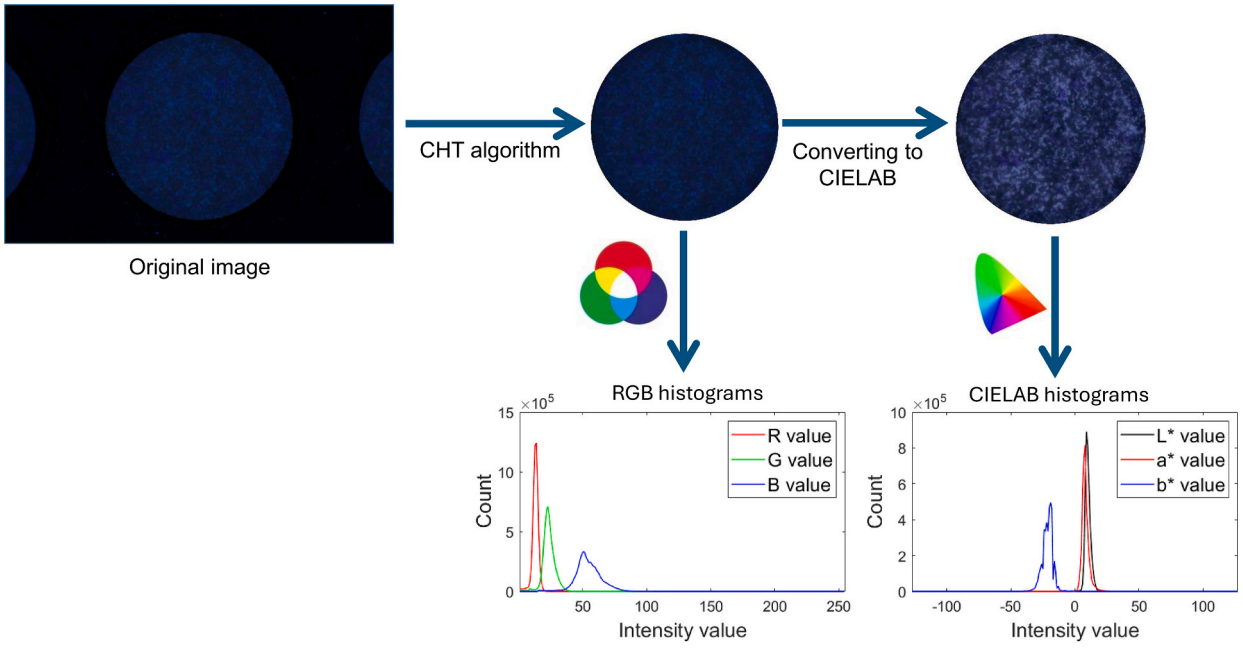

Fig. 2. Main steps of the image analysis workflow, including tablet detection using the circle Hough Transform (CHT), colour feature extraction in the RGB colour space, and subsequent conversion to the CIELAB colour space.

the network from relying excessively on noisy or unrepresentative training samples (Burden and Winkler, 2008).

The optimal number of hidden neurons was determined by training models with 1 to 10 neurons, each configuration being trained 30 times. To account for the variability introduced by random data splitting and the initialization of weights and biases (Nguyen-Widrow method), a bootstrap resampling approach was used. The number of tablets was small relative to the number of potential network parameters; therefore, architectures with a single hidden layer and a restricted number of neurons (1–10) were deliberately selected to limit model complexity.

A total of 200 resampling iterations were carried out, each involving random partitioning of the dataset and independent model training. This procedure allowed for a more reliable estimation of model performance by accounting for variability due to data selection and network initialization. During the training procedure, the mean squared error (MSE) was used as the performance function within the Bayesian regularization, while model performance was evaluated using root mean squared error (RMSE) value. RMSE was calculated with the following equation (Eq. 1):

$$RMSE = \sqrt{\frac{1}{n}\sum_{t=1}^{n}(R_t - T_t)^2} \tag{1}$$

The measured and the predicted dissolution curves were compared using f_1 and f_2 values (Muselík et al., 2021). The f_1 difference factor determines the average percentage difference between two dissolution profiles (Eq. 2):

$$f_1 = 50log_{10}\left\{\left[\sum_{t=1}^{n}|R_t - T_t|\right] / \left[\sum_{t=1}^{n}R_t\right]\right\} \times 100 \tag{2}$$

where n represents the number of points in the dissolution curve, R_t and T_t are the measured and predicted dissolution values at time t. Lower f_1 values indicate greater similarity between the profiles.

The f_2 similarity factor was calculated according to the following formula (Eq. 3):

$$f_2 = 50log_{10}\left\{\left[1 + \frac{1}{n}\sum_{t=1}^{n}w_t(R_t - T_t)^2\right]^{0.5} \times 100\right\} \tag{3}$$

where w_t is an optional weighting factor, which was not used in this study. Only one point beyond 85% dissolution was included in the calculations to limit the influence of the plateau region, which could undeservingly improve the results. The f_2 value ranges from 0 to 100, with higher values indicating greater similarity between dissolution profiles.

Model evaluation was performed using two independent datasets that were not included in model generation procedure, consisting of the external validation samples produced in non-continuous mode and the external test samples obtained in continuous mode.

3. Results and discussion

3.1. In vitro dissolution profiles of the tablet formulations

The average dissolution profiles for formulations containing 5% to 35% HPMC are shown in Fig. 3. As expected with hydrophilic matrix systems, tablets with lower HPMC content released the API more rapidly, reaching near-complete dissolution within 100 min. In contrast, higher HPMC concentrations led to delayed drug release; the formulation containing 35% HPMC reached complete dissolution at 300 min. The slower release observed at higher HPMC levels can be attributed to the formation of a swollen polymer layer upon contact with the dissolution medium, which acts as a barrier to drug diffusion. This hydrated layer regulates the rate at which the API is released, resulting in a more gradual and controlled dissolution profile (Maderuelo et al., 2011).

HPMC is known to exhibit pronounced feeding variability in continuous manufacturing, where even short-term deviations or material spikes in the feeder can lead to concentration shifts and out-of-specification products (Allenspach et al., 2021). Our results demonstrate that even 5% change in the HPMC content produced clearly distinguishable dissolution curves, as indicated by the distinct profiles and their corresponding standard deviations in Fig. 3. Such a controlled trend was essential for evaluating whether image-derived features, and subsequently the ANN models were capable of capturing formulation-related differences in release behaviour.

In the present study, blend uniformity was not explicitly analysed and minor fluctuations during blending and tableting cannot be fully excluded. However, the final dissolution rates of tablets prepared from the same formulation exhibited limited tablet-to-tablet variability, as shown in Fig. 3, indicating that any fluctuations in API content were

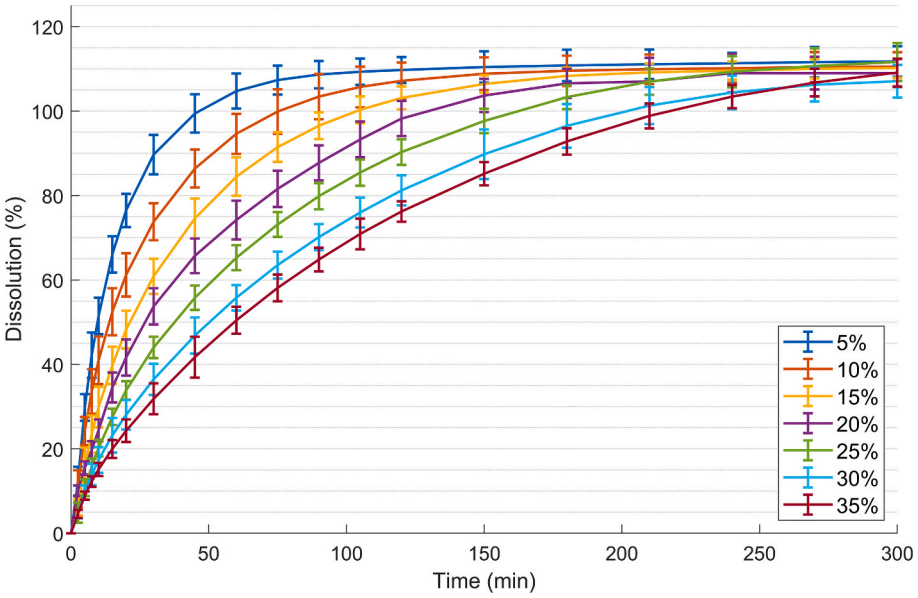

Fig. 3. Mean dissolution curves of the tablet formulations containing different HPMC concentrations. Data are presented of 10 samples for each formulation ± standard deviation.

small. Anhydrous caffeine and dibasic calcium phosphate were initially blended using a multifunctional continuous twin-screw blender, as preliminary experiments without this step resulted in pronounced variability in the dissolution profiles for samples prepared from the same formulation. The application of the twin-screw blending step substantially reduced this variability, leading to more consistent dissolution behaviour. In addition, tablet homogeneity was qualitatively assessed by visual inspection of the UV images, which provide spatial information related to the surface. Accordingly, the Supplementary Material includes a comparison between a tablet prepared from a properly blended formulation and a deliberately inhomogeneous tablet (Fig. S1).

3.2. Acquired UV images and image processing

The HPMC-containing tablets exhibited a distinct blue coloration when exposed to UV illumination at ~ 270 nm (Fig. S1a). To examine this behaviour in more detail, fluorescence spectroscopy was performed (Fig. 4). When HPMC is excited at a wavelength of ~ 270 nm, it exhibits fluorescence in the blue range (approximately 330–380 nm). Intrinsic photoluminescence has been reported for polycarbohydrates such as starch and cellulose, which, despite the lack of aromatic chromophores, contain a high density of electron-rich oxygen atoms. In the solid or aggregated state, close packing of polymer chains enables clustering of these oxygen atoms, promoting electron delocalization. Similar effects have been observed for other carbohydrate aggregates, such as sodium alginate, chitosan, glucose, xylose, and cyclodextrin, suggesting this is a characteristic of carbohydrates (Chen and Yuan, 2025). Accordingly, an increase in HPMC content would be expected to result in a corresponding increase in the blue coloration observed under UV illumination.

Fig. 5 depicts two UV images of tablets containing the lowest (5%) and the highest (35%) HPMC concentration, alongside a comparison of their CIELAB and RGB colour component histograms. Under visible light, the tablets appeared identical and no visible differences where visible on their surfaces. Under UV illumination, however, clear differences emerge: tablets with higher HPMC content display larger and more intense light-blue regions, whereas those with lower HPMC levels appear darker and less heterogeneous. Because all other excipients were kept constant, these differences are attributable to the varying HPMC concentration. It can be concluded that the HPMC contributed a stronger UV-induced signal than the other components.

The comparison of the extracted colour components could reveal trends associated with varying HPMC content. As expected from the visual evaluation, the L* (lightness) and R (red) values remained similar across the two formulations (Fig. 5cd), indicating minimal influence of HPMC concentration on overall brightness and red intensity under UV illumination. In contrast, the a* (green–red axis) and G (green) values showed a noticeable shift toward higher values (Fig. 5ef), accompanied by broader histograms. This suggests an increase in the green component in the UV images with higher HPMC levels. Similarly, both b* and B values shifted toward higher values (Fig. 5gh), consistent with increased fluorescence of HPMC. These changes in the colour distribution, particularly in the a*, b*, G, and B channels, provide a basis for differentiating between tablet formulations using UV images and were selected as potential input variables for subsequent dissolution prediction using ANNs. The preprocessed histograms averaged by class are presented in the supplementary material (Fig. S2, Fig. S3). Normalization and mean centering were applied to the histograms prior to their use as ANN inputs.

3.3. Training and evaluation of ANN models for in vitro dissolution prediction

In this work, traditional image analysis was used to extract features from the images, which were then used as input for the ANN models to predict dissolution profiles. CNNs provide an alternative approach for image-based modelling through the identification of relevant spatial features within image data. Galata et al. utilized a CNN-based approach using Raman and NIR chemical imaging to predict dissolution profiles of extended release tablets containing HPMC without intermediate image analysis step. Each tablet was represented by an HPMC concentration map of 31 × 31 pixels (Raman) or 48 × 48 pixels (NIR), which served as the direct input to the CNN (Galata et al., 2023). However, in the present study, the acquired images were substantially larger, therefore CNN-based modelling would be very computationally demanding and unfeasible on regular computers. Therefore in this study, image processing was applied to drastically reduce the size of the data fed into the neural network models. Accordingly, the modelling approach adopted in this work was based on extracted image features rather than direct use of the image data, and these features were used as inputs to the ANN models to predict the dissolution profiles.

Seven ANN models were developed to explore the feasibility of predicting dissolution profiles based on selected colour components extracted from UV images. Table 2 summarizes the input data, the applied histogram ranges, and the optimal number of hidden neurons.

ANN1 and ANN2 utilized individual RGB components as input, which were then transformed and reduced to five PCs. ANN3 also used the B channel, but without PCA, relying directly on a selected histogram

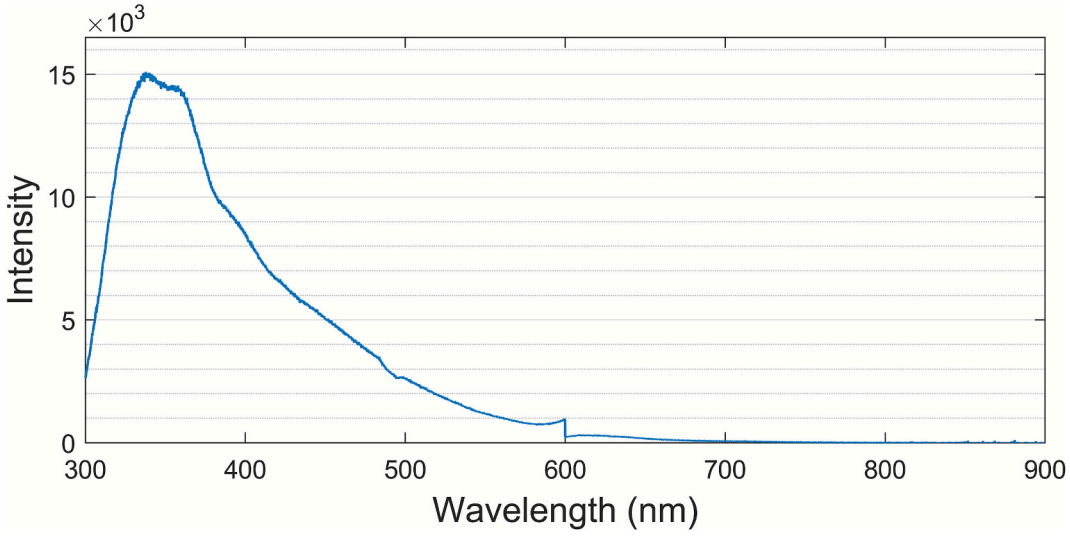

Fig. 4. Fluorescent spectra of HPMC at the excitation wavelength of 270 nm.

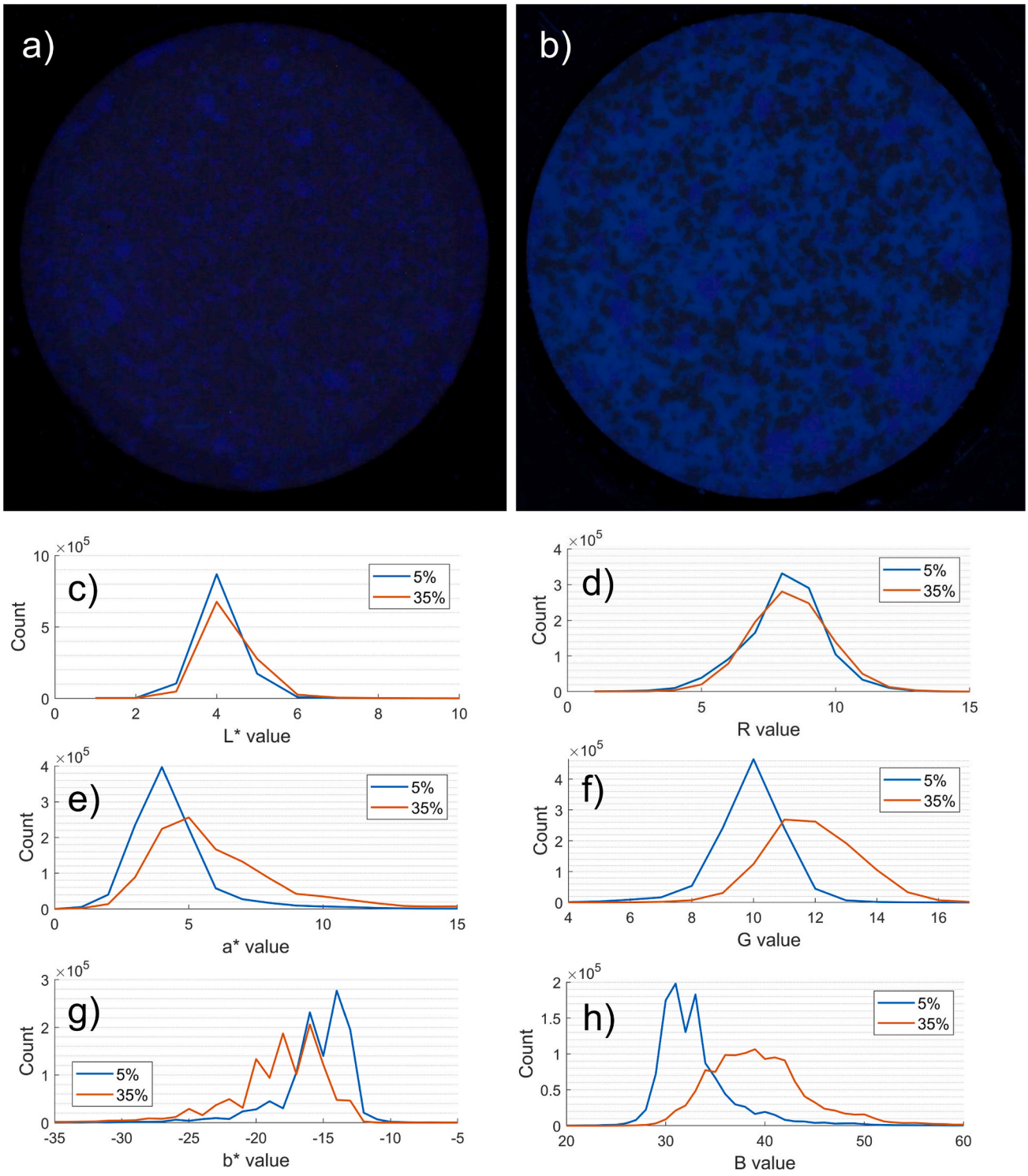

Fig. 5. Comparison of UV images of tablets containing 5% (a) and 35% (b) HPMC, along with corresponding CIELAB colour components: L* (c), a* (e), b* (g), and RGB channels: R (d), G (f), and B (h). Image brightness was adjusted for better visualization.

range to compare PCA-based feature compression with raw input descriptors. ANN4 combined the G and B channels by applying PCA independently to each channel to reduce dimensionality and then merging the resulting PCs from both channels to form a combined input vector for the model. ANN5 and ANN6 used the individual a* and b* channels from the CIELAB colour space, while ANN7 incorporated both colour components, with five PCs selected from each channel. Table S1 in the Supplementary material summarizes the variance associated with the selected PCs for each colour component.

The optimal number of hidden neurons was determined individually for all models by systematically training networks with 1–10 neurons. Models with one to three hidden neurons demonstrated stronger predictive accuracy. This observation is consistent with the findings of Péterfi et al., who reported that ANN models based on Raman and NIR spectra achieved the best performance with a similarly low number of neurons (Péterfi et al., 2023). This suggests that the relationship between input features and dissolution behaviour may be captured by a relatively simple function that requires only a few neurons in the ANN.

Table 2
Input data for the ANN models and the optimal number of hidden neurons.

ANN model	*Colour component*	*Range (bin values)*	*Number of PCs*	*Optimal neuron number*
ANN1	G (from RGB)	5 to 17	5	2
ANN2	B (from RGB)	22 to 55	5	1
ANN3	B (from RGB)	22 to 55	– #	1
ANN4	G and B (from RGB)	5 to 17 (G value) 22 to 55 (B value)	5 + 5	1
ANN5	a* (from Lab)	1 to 15	5	1
ANN6	b* (from Lab)	−30 to −10	5	3
ANN7	a* and b* (from Lab)	1 to 15 (a value) −30 to −10 (b value)	5 + 5	1

Principal component analysis was not applied.

As the input dimensionality of the PCA-based models was limited to a few descriptors, larger network architectures were not expected to provide additional modelling capability.

The performance of the seven ANN models was evaluated and compared using the RMSE metrics on both the training and external validation datasets, as summarized in Table 3. The f_1 and f_2 values were used to compare the measured dissolution profiles with those predicted by the ANN models. The distribution of the mentioned values are presented in the box plots of Fig. 6 for the samples of the external validation set. The measured and predicted dissolution curves for these tablets are available in the supplementary material (fig. S4, fig. S5).

All models yielded average f_2 values above the regulatory threshold of 50 (Hoffelder, 2018), indicating that each model was able to predict dissolution profiles with acceptable similarity to the reference. However, the distribution of the performance metrics revealed clear differences in robustness. In particular, ANN1 and ANN4 produced certain predictions with f_2 values below 50 for some validation samples, reflecting lower performance when input channels showed only minor variation across formulations. In Fig. 6c, ANN1, ANN4 and ANN7 show outliers at higher RMSE values, indicating that although their average RMSE values are moderate, certain validation cases resulted in substantially larger prediction errors. The presence of such outliers highlights differences in generalization behaviour that are not evident from average performance values alone. This was therefore taken into account during model evaluation to obtain a more complete picture of model behaviour across the external validation samples. In this context, ANN models showing fewer outliers were considered more reliable.

The box plots also highlight differences in variability, with ANN2 and ANN3 having the narrowest interquartile ranges for the evaluation metrics, meaning their prediction errors were more consistent across the validation samples. In contrast, some other models had wider ranges, suggesting that in certain cases the predictions were closer to the measured, while in others they deviated more strongly. The models that utilized the B channel in the RGB space and the b* component in the CIELAB space yielded the best predictions, which is consistent with the observations mentioned in Section 3.2.

Table 3
F_1, f_2 and RMSE values for ANN-based dissolution predictions of the training and external validation datasets.

Model name	*Train f_1*	*Train f_2*	*Train RMSE [%]*	*Valid f_1*	*Valid f_2*	*Valid RMSE [%]*
ANN1	7.15	70.43	4.36	8.22	71.25	4.29
ANN2	3.76	80.51	2.35	4.36	80.68	2.34
ANN3	3.53	82.60	2.06	4.68	80.28	2.40
ANN4	6.79	71.02	4.31	6.69	75.32	3.57
ANN5	7.34	70.54	4.58	9.18	68.35	4.67
ANN6	6.91	71.28	4.29	7.69	71.85	3.92
ANN7	5.71	73.64	3.26	7.74	72.33	3.98

Among the models, ANN2 and ANN3 demonstrated the most favorable predictive performance, with validation RMSE of 2.34% and 2.40%, respectively, and f_2 values of 80.68 and 80.28, while the CIELAB-based models (ANN5–ANN7) showed lower overall performance. ANN5, which relied solely on the a* component, showed the weakest performance, yielding the highest RMSE (4.67%) and the lowest f_2 value (68.35). ANN7, which combined both a* and b* components, outperformed the single-channel CIELAB models, although it still remained inferior to the B-based RGB models.

To further investigate model behaviour, the f_2 similarity factor was evaluated separately for each formulation subset. This allows a more detailed assessment of how the ANN models perform across formulations with different HPMC contents, rather than relying only on overall average values. As shown in Fig. 7, most models exhibited their lowest average f_2 values for the 7.5% HPMC formulation, whereas the highest f_2 values were obtained for the 32.5% HPMC formulation. The lower the HPMC content, the faster the dissolution, and the early phase of these profiles typically shows higher variability. For the 7.5% HPMC tablets, 85% release was reached earlier, resulting in fewer data points being included in the f_2 calculation. As a result, variability in the initial phase had a greater impact on the f_2 values, which may explain the lower f_2 values observed for this subgroup. Some models, particularly ANN5, showed reduced predictive accuracy for the dissolution behaviour of the 7.5% HPMC formulations. Some of the observed differences may also reflect limitations of certain models in capturing this increased variability, which could potentially be mitigated by increasing the amount of training data for the 7.5% HPMC formulations. Among the evaluated models, ANN2 and ANN3 achieved similarly high f_2 values across all three formulations. This suggests that these models captured formulation-dependent behaviour more consistently than the other network configurations. Average f_1 and RMSE values for the different ANN models, calculated separately for the three formulation subsets, are presented in the Supplementary material (Fig. S6 and Fig. S7).

Additional insight into model behaviour is provided by the residual analysis presented in the Supplementary material (Fig. S8). While some models exhibit asymmetric residual distributions, indicating unevenly distributed prediction errors across the dissolution profiles, ANN2 and ANN3 show narrower and more symmetric residual histograms centred around zero. This is consistent with their higher and more uniform f_2 values and suggests more balanced predictive performance.

Other studies predicting dissolution behaviour of HPMC-containing tablets have reported a wide range of f_2 values, reflecting differences in both modelling approach and input data. Zeng et al. studied tablets prepared with varying process settings and formulation factors such as API and HPMC content. Their reported PLS models based on Raman mapping achieved an average f_2 of 79.76 (Zeng et al., 2022). Horkovics-Kovats et al. prepared tablets with varying API and HPMC concentrations and proposed a deterministic permeation model that combined Raman spectra with compression data, yielding an average f_2 of 71.53 (Horkovics-Kovats et al., 2022). Galata et al. applied Raman imaging to characterise HPMC concentration and particle size in sustained-release tablets and used these data as inputs for convolutional neural network models, resulting in an average f_2 of 62.7 (Galata et al., 2023). The predictive performance of the ANN models presented here was therefore comparable to values reported for both data-driven and mechanistic approaches in the literature.

3.4. An application example of the selected model

Since ANN2 and ANN3 performed comparably, ANN2 was selected as the final model due to its lower input dimensionality resulting from PCA compression. This model was subsequently used to predict the dissolution profiles of tablets of the external test set produced with the tabletpress operated in continuous mode.

The smaller input size allows both training and prediction to be

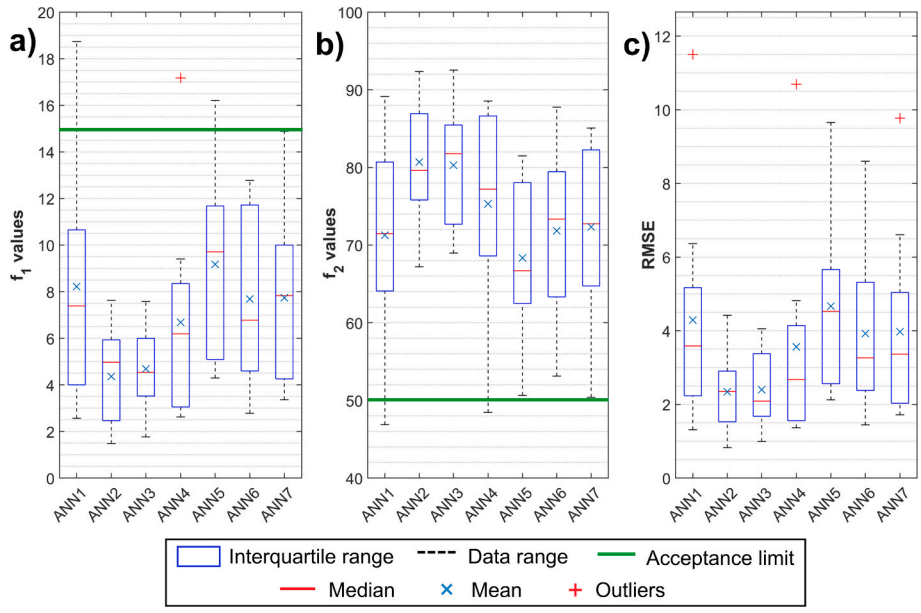

Fig. 6. Statistical distribution of the f_1 values (a), f_2 values (b) and RMSE values (c) for the external validation sample prepared in non-continuous mode. Results are shown for three formulations (7.5%, 20%, and 32.5% HPMC), with three tablets analysed per formulation (total n = 9 tablets).

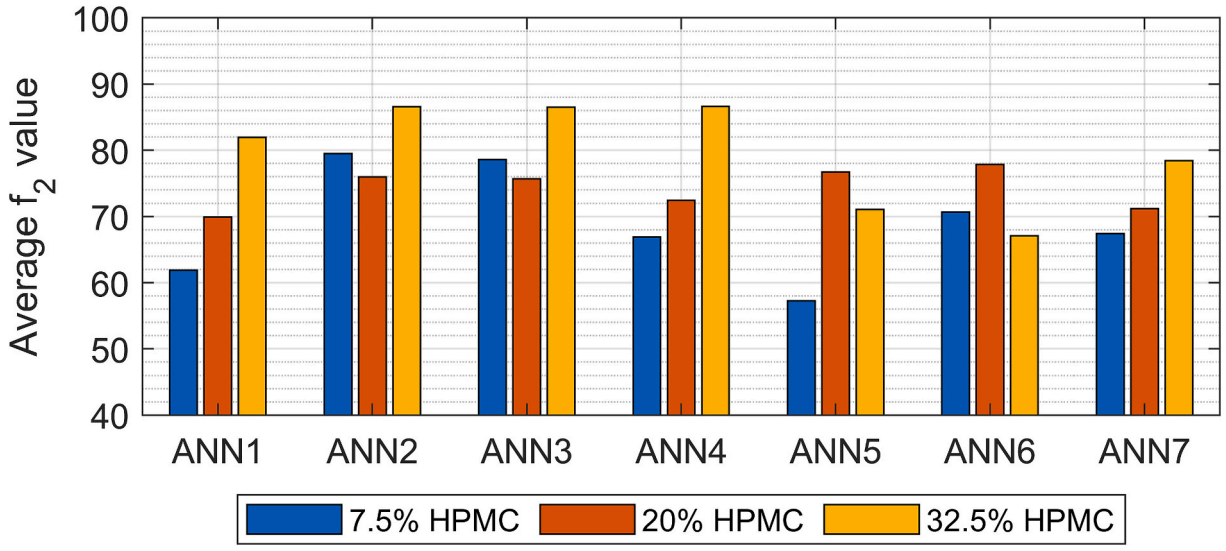

Fig. 7. Average f_2 similarity factors for the different ANN models, calculated separately for the three formulation subsets.

faster, which is especially valuable when models are intended for feedback control and continuous manufacturing. Industrial implementations involving high sample throughput require greater computational demands, and a reduced input size helps maintain manageable processing times under these conditions. The external test set allowed to evaluate the performance of ANN2 to be assessed under dynamic composition shift.

ANN2 was then evaluated, with the primary aim of assessing whether UV imaging-based data could support dissolution prediction. The final model was applied to the tablets produced in continuous mode, and dissolution profiles were predicted for all 500 tablets obtained during the process. The experiment started with the 20% HPMC blend. When the initial powder mixture was nearly depleted, the 32.5% HPMC blend was added at tablet 150, followed by the 7.5% HPMC blend at tablet 323. Because each new blend was added on top of the remaining powder, the transition between formulations could be either gradual or abrupt, depending on how the powders mixed in the feeder.

To provide an overview of the entire batch, Fig. 8 presents the predicted dissolved caffeine amount at 60 min for all 500 tablets. Red dots mark the measured values for the 12 tablets that were tested *in vitro*. The 60-minute time point provided the greatest discrimination among the formulations during the dissolution test. The predicted concentrations reflected the formulation changes during the experiment in continuous mode. The amount of dissolved API decreased after the introduction of the 32.5% blend, consistent with a slower drug release, and increased again after the switch to the 7.5% blend, where the lower HPMC content led to faster dissolution and higher API levels at 60 min. The measured values of the 12 tablets showed similar trends and corresponded closely with the predicted values.

During the transition from the 20% to the 32.5% HPMC formulation, the predicted dissolved API indicates a gradual decrease, which is consistent with the presence of residual powder from the previous blend in the feeder. By contrast, the introduction of the 7.5% HPMC formulation produced a sharp change, with the predicted values rising more

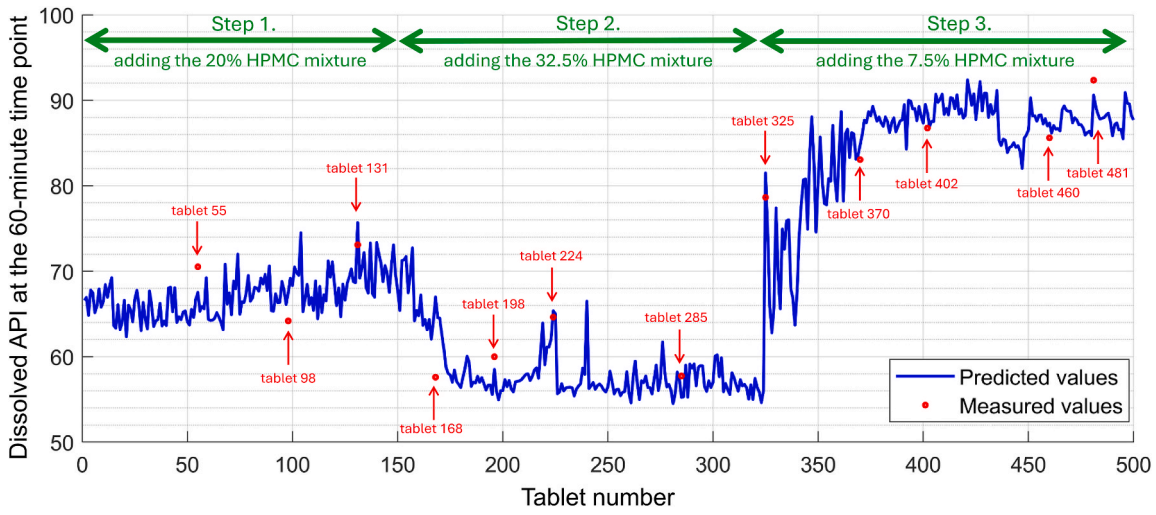

Fig. 8. Predicted and measured dissolved API values at the 60-minute time point for tablets produced in continuous mode.

abruptly. These differences between gradual and abrupt transitions illustrate how process conditions influenced dissolution outcomes and how the model was able to capture these effects across the entire batch. This is important for continuous manufacturing scenarios, where such shifts directly influence tablet quality.

Fig. 9 shows the predicted and measured curves of the 12 tablets,

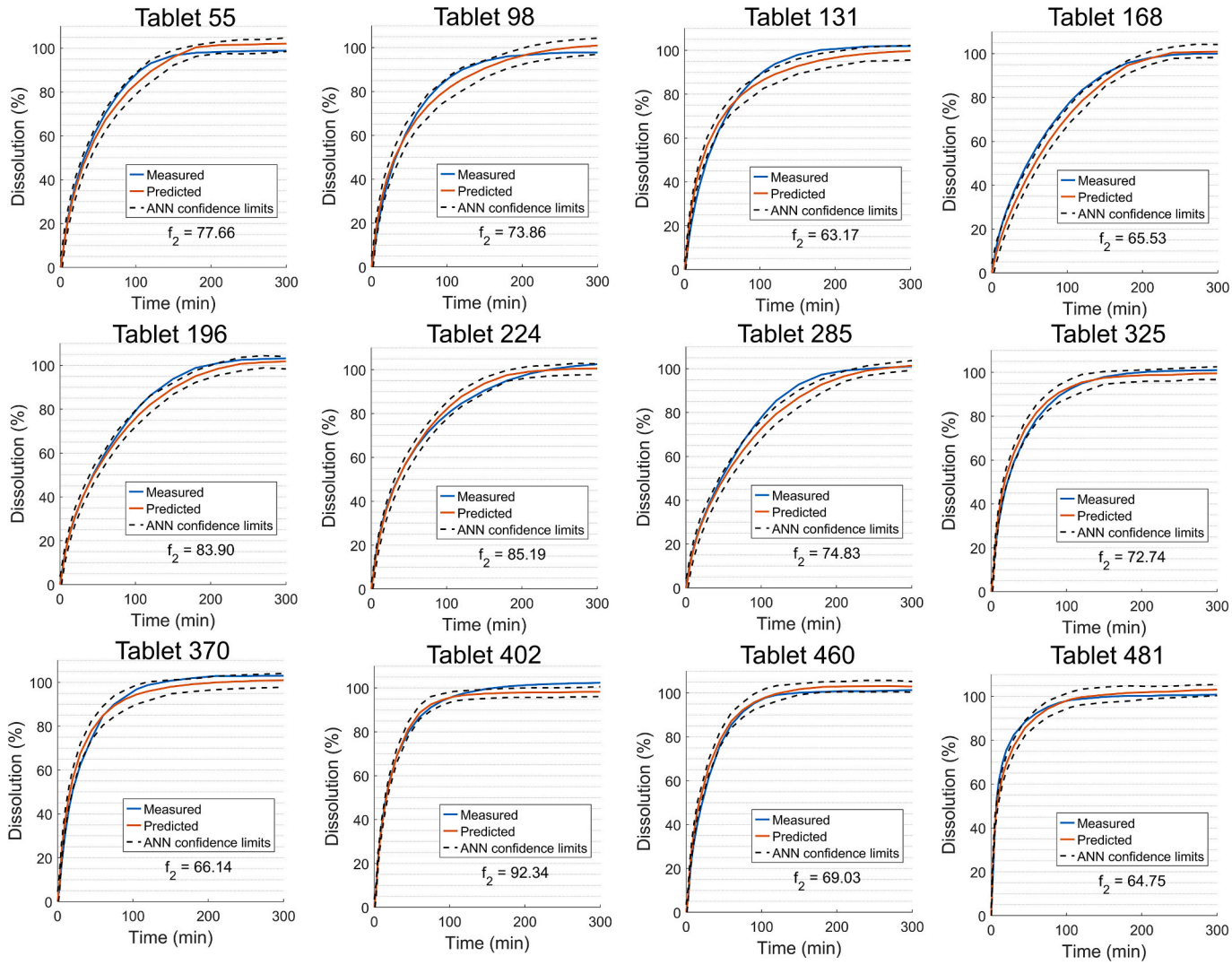

Fig. 9. Measured and predicted dissolution profiles of the 12 tablets from the external test set.

which followed similar trends. The predicted curves captured both the overall shape of the dissolution profiles and the differences in dissolution rate between formulations. All of the calculated f_2 values were above 60, indicating a high similarity between the predicted and measured profiles. The average f_2 value was 74.09, the average f_1 value was 6.33, and the RMSE was 3.38%. These values demonstrate that the model maintained acceptable predictive performance even under conditions where the formulation composition changed dynamically. Some of the tablets (most notably tablets 131, 285 and 402) were associated with measured dissolution profile falling outside the confidence interval of the ANN prediction. This can be attributed to the relatively narrow confidence interval, which means that during the bootstrap sampling, the models consistently yielded predicted dissolution profiles with only minor variation between individual predictions. Thus, due to the narrowness of the confidence interval, values that fall slightly outside its limits do not necessarily indicate large deviations. Moreover, most of these deviations occur above 85% of the dissolution, and consequently, they are not taken into account when calculating the f_2 value. This is because the f_2 value is concerned with the initial part of the curve and penalizes inaccuracies in the earlier phases of the dissolution profile. Tablets produced during the transitional phase between formulations, such as tablets 168 and 325, were predicted with similar performance to the rest of the tablets. This shows that the method is capable of giving reliable predictions for the whole process, including transition regions.

Although the present study did not implement real-time prediction, the ability to handle large numbers of samples rapidly highlights the potential of such systems for monitoring and supporting control strategies in continuous manufacturing. However, current implementation presents a feasibility testing, previous studies have demonstrated that UV imaging has great potential for in-line monitoring of pharmaceutical products (Ficzere et al., 2025). The integration of dissolution prediction into such a framework adds a further dimension to quality monitoring.

Although flat-faced punches were used in the present study, the UV imaging-based approach is not restricted to this tablet geometry. For biconvex tablets, the primary challenge arises from the limited depth of field, as tablet curvature can make it difficult to keep the entire tablet surface in focus. However, with the use of appropriate imaging conditions, including adjustment of the field of focus and depth of field, the method can be extended to tablets manufactured with concave punches. Previous studies have successfully applied UV/VIS imaging to biconvex tablets for API content determination in amlodipine and valsartan tablet formulations (Ficzere et al., 2024).

It should be noted that the applicability of the presented method depends on the visual appearance of the API and excipients in the analysed formulation. The main criterion is that under the utilized illumination the compound of interest (be it the API or an excipient that determines the rate of dissolution) should be distinguishable from the other components. In the case of excipients, further studies should focus on quantifying compounds that affect the drug release profile of tablets, such as disintegrants or matrix polymers for controlled release. If sufficient contrast is not achieved under the current illumination type, measurements at multiple UV wavelengths or the use of a UV-sensitive camera may be required. However, there will inevitably be API-excipient combinations where the application of the presented method could be challenging due to insufficient contrast under the available illumination wavelengths. The applicability of the proposed approach can be assessed rapidly, as several test images are sufficient to verify whether adequate optical contrast exists between the API and excipients.

Regarding the broader application of the proposed technique, several limitations need to be addressed. Similar to most data-driven models, the ANNs presented in this work can only work reliably with this specific formulation. Substantial changes to the composition or manufacturing parameter of the tablets will, in most cases, result in inaccurate predictions unless the ANN is retrained. There are some minor changes that would potentially not affect model performance, such as using a different grade of filler material. The same ANN model will likely not work for similar tablets with a different API due to the potential visual changes and different solubility of the drug resulting in changes of the drug release rate. Using a different grade of HPMC is expected to affect model performance, because the same HPMC concentration will yield different dissolution profiles. Changing the compression force or tablet geometry will also alter the dissolution, although the changes are typically smaller compared to those caused by using a different grade of HPMC. The proposed system however is intended for formulations composed of a fixed set of component types. In this context, the aforementioned changes are unlikely to occur due to the immense regulatory burden of modifying an already registered formulation. Nevertheless, the system could also be applied as a prescreening tool during supplier changes to assess whether excipients or active pharmaceutical ingredients from a new source result in comparable dissolution behaviour. When applying a model across different HPMC grades, key polymer descriptors such as molecular weight and degree of substitution can be included as additional input variables; however, the model must also be trained using data from different HPMC grades to learn how variations in polymer properties influence the dissolution curve (Galata et al., 2021). Similarly, compression force data measured during tableting can also be included as an additional input variable in the ANN model, to reflect the influence of compression force on dissolution behaviour.

The results of the current study demonstrate that UV imaging can also generate input data suitable for predicting tablet dissolution behaviour. With image-based prediction, large numbers of tablets could be analysed rapidly, enabling the detection of critical changes in product quality during manufacturing. Capturing tablet-to-tablet variability is especially important in pharmaceutical manufacturing, since even small differences between tablets can affect dissolution behaviour and, ultimately, product performance. This approach could provide a more detailed understanding of product performance and enables the early identification of out-of-specification tablets. Integration of dissolution prediction into process monitoring has the potential to improve quality assurance in tablet manufacturing in the future.

4. Conclusion

In this study, UV imaging was used to predict the dissolution behaviour of extended-release tablets containing different levels of HPMC. ANN models were trained using image-derived colour features, and their predictive ability was evaluated against measured dissolution profiles.

All models achieved average f_2 values above 60, and the most accurate results were obtained for the model using the B channel of the RGB colour space, which showed an average f_2 of 80.68 for the external validation sample set. The model successfully captured formulation changes while the tablet press was operated continuously, and the predicted dissolution profiles reflected the differences in the HPMC content. When applied to tablets of the external test set, the ANN model provided predictions with an average f_2 of 74.09.

The results demonstrate that UV imaging can provide valuable information related to HPMC content, enabling ANN-based prediction of dissolution performance. The method detected formulation changes during production, demonstrating the models' ability to respond to variability affecting product performance. Detection of deviations in release behaviour allows potential root causes, which can then be minimised through the adjustment of relevant process parameters.

Future studies should also investigate the integration of machine vision systems directly into the production line, allowing dissolution behaviour to be determined during manufacturing experiments. Coupled with a feedback control system, process parameters can be adjusted if deviations compromise quality, and coupled with an ejection system, tablets that do not meet regulatory standards could be removed. Together, these measures would enhance patient safety, reduce batch rejections and associated costs, increase manufacturing efficiency, and

could strengthen overall product quality assurance.

CRediT authorship contribution statement

Orsolya Péterfi: Writing – review & editing, Writing – original draft, Visualization, Software, Investigation, Data curation. **Lilla Alexandra Mészáros:** Writing – review & editing, Software, Methodology, Formal analysis. **Bence Szabó-Szőcs:** Methodology, Investigation. **Máté Ficzere:** Methodology, Investigation. **Brigitta Nagy:** Writing – review & editing, Software, Methodology, Formal analysis. **Emese Sipos:** Supervision. **Sándor Lenk:** Formal analysis, Investigation, Validation. **Zsombor Kristóf Nagy:** Writing – review & editing, Supervision, Resources, Methodology, Funding acquisition, Conceptualization. **Dorián László Galata:** Writing – review & editing, Writing – original draft, Supervision, Methodology, Investigation, Formal analysis.

Declaration of competing interest

The authors declare that they have no known competing financial interests or personal relationships that could have appeared to influence the work reported in this paper.

Acknowledgements

The project was supported by the European Union project RRF-2.3.1–21–2022–00004 within the framework of the Artificial Intelligence National Laboratory. Further support was received by the János Bolyai Research Scholarship of the Hungarian Academy of Science. The project supported by the Doctoral Excellence Fellowship Programme (DCEP) is funded by the National Research Development and Innovation Fund of the Ministry of Culture and Innovation and the Budapest University of Technology and Economics, under a grant agreement with the National Research, Development and Innovation Office. This project has received funding from the European Union's Horizon Europe research and innovation programme under the Marie Skłodowska-Curie grant agreement No 101207440.

Appendix A. Supplementary data

Supplementary data to this article can be found online at https://doi.org/10.1016/j.ijpharm.2026.126649.

Data availability

Data will be made available on request.

References

Allenspach, C., Timmins, P., Lumay, G., Holman, J., Minko, T., 2021. Loss-in-weight feeding, powder flow and electrostatic evaluation for direct compression hydroxypropyl methylcellulose (HPMC) to support continuous manufacturing. Int. J. Pharm. 596, 120259. https://doi.org/10.1016/j.ijpharm.2021.120259.

Azarmi, S., Roa, W., Löbenberg, R., 2007. Current perspectives in dissolution testing of conventional and novel dosage forms. Int. J. Pharm. 328, 12–21. https://doi.org/10.1016/j.ijpharm.2006.10.001.

Baghel, S., Cathcart, H., O'Reilly, N.J., 2018. Investigation into the solid-state properties and dissolution profile of spray-dried ternary amorphous solid dispersions: a rational step toward the design and development of a multicomponent amorphous system. Mol. Pharm. 15, 3796–3812. https://doi.org/10.1021/acs.molpharmaceut.8b00306.

Bawuah, P., Markl, D., Turner, A., Evans, M., Portieri, A., Farrell, D., Lucas, R., Anderson, A., Goodwin, D.J., Zeitler, J.A., 2021. A fast and non-destructive terahertz dissolution assay for immediate release tablets. J. Pharm. Sci. 110, 2083–2092. https://doi.org/10.1016/j.xphs.2020.11.041.

Beg, S., Hasnain, M.S., Rahman, M., Swain, S., 2019. Introduction to Quality by Design (QbD): fundamentals, principles, and applications, pharmaceutical quality by design. Elsevier Inc., 10.1016/b978-0-12-815799-2.00001-0.

Bharate, S.S., 2021. Recent developments in pharmaceutical salts: FDA approvals from 2015 to 2019. Drug Discov. Today 26, 384–398. https://doi.org/10.1016/j.drudis.2020.11.016.

Brands, R., Tebart, N., Thommes, M., Bartsch, J., 2023. UV/Vis spectroscopy as an in-line monitoring tool for tablet content uniformity. J. Pharm. Biomed. Anal. 236, 115721. https://doi.org/10.1016/j.jpba.2023.115721.

Burden, F., Winkler, D., 2008. Bayesian Regularization of Neural Networks. pp. 23–42. Doi:10.1007/978-1-60327-101-1_3.

Chavez, P.-F., Sacré, P.-Y., De Bleye, C., Netchacovitch, L., Mantanus, J., Motte, H., Schubert, M., Hubert, P., Ziemons, E., 2015. Active content determination of pharmaceutical tablets using near infrared spectroscopy as Process Analytical Technology tool. Talanta 144, 1352–1359. https://doi.org/10.1016/j.talanta.2015.08.018.

Chen, X., Yuan, W.Z., 2025. Clustering-Triggered Emission in Nonaromatic Polymers, in: Encyclopedia of Aggregation-Induced Emission. Springer Nature Singapore, Singapore, pp. 1–12. Doi:10.1007/978-981-97-1574-9_8-1.

Chu, K.R., Lee, E., Jeong, S.H., Park, E.-S., 2012. Effect of particle size on the dissolution behaviors of poorly water-soluble drugs. Arch. Pharm. Res. 35, 1187–1195. https://doi.org/10.1007/s12272-012-0709-3.

Ferdoush, S., Gonzalez, M., 2024. A two-stage mechanistic reduced-order model of pharmaceutical tablet dissolution: population balance modeling and tablet wetting functions. Int. J. Pharm. 664, 124635. https://doi.org/10.1016/j.ijpharm.2024.124635.

Ficzere, M., Alexandra Mészáros, L., Diószegi, A., Bánrévi, Z., Farkas, A., Lenk, S., László Galata, D., Kristóf Nagy, Z., 2024. UV imaging for the rapid at-line content determination of different colourless APIs in their tablets with artificial neural networks. Int. J. Pharm. 657, 124174. https://doi.org/10.1016/j.ijpharm.2024.124174.

Ficzere, M., Diószegi, A., Farkas, A., Weiss, B., Mészáros, L.A., Nagy, Z.K., 2025. High throughput in-line content uniformity measurement of tablets based on real-time UV imaging. Int. J. Pharm. 669, 125066. https://doi.org/10.1016/j.ijpharm.2024.125066.

Fink, E., Celikovic, S., Martins Fraga, R., Remmelgas, J., Rehrl, J., Khinast, J., 2024. In-line porosity and hardness monitoring of tablets by means of optical coherence tomography. Int. J. Pharm. 666, 124808. https://doi.org/10.1016/j.ijpharm.2024.124808.

Galata, D.L., Farkas, A., Könyves, Z., Mészáros, L.A., Szabó, E., Csontos, I., Pálos, A., Marosi, G., Nagy, Z.K., Nagy, B., 2019. Fast, spectroscopy-based prediction of in vitro dissolution profile of extended release tablets using artificial neural networks. Pharmaceutics 11, 1–18. https://doi.org/10.3390/pharmaceutics11080400.

Galata, D.L., Gergely, S., Nagy, R., Slezsák, J., Ronkay, F., Nagy, Z.K., Farkas, A., 2023. Comparing the performance of Raman and near-infrared imaging in the prediction of the in vitro dissolution profile of extended-release tablets based on artificial neural networks. Pharmaceuticals 16, 1243. https://doi.org/10.3390/ph16091243.

Galata, D.L., Könyves, Z., Nagy, B., Novák, M., Mészáros, L.A., Szabó, E., Farkas, A., Marosi, G., Nagy, Z.K., 2021. Real-time release testing of dissolution based on surrogate models developed by machine learning algorithms using NIR spectra, compression force and particle size distribution as input data. Int. J. Pharm. 597, 11. https://doi.org/10.1016/j.ijpharm.2021.120338.

Guiastrennec, B., Söderlind, E., Richardson, S., Peric, A., Bergstrand, M., 2017. In vitro and in vivo modeling of hydroxypropyl methylcellulose (HPMC) matrix tablet erosion under fasting and postprandial status. Pharm. Res. 34, 847–859. https://doi.org/10.1007/s11095-017-2113-7.

Hernandez, E., Pawar, P., Keyvan, G., Wang, Y., Velez, N., Callegari, G., Cuitino, A., Michniak-Kohn, B., Muzzio, F.J., Romañach, R.J., 2016. Prediction of dissolution profiles by non-destructive near infrared spectroscopy in tablets subjected to different levels of strain. J. Pharm. Biomed. Anal. 117, 568–576. https://doi.org/10.1016/j.jpba.2015.10.012.

Hoffelder, T., 2018. Comparison of dissolution profiles: a statistician's perspective. Ther. Innov. Regul. Sci. 52, 423–429. https://doi.org/10.1177/2168479017749230.

Horkovics-Kovats, S., László Galata, D., Zlatoš, P., Nagy, B., Alexandra Mészáros, L., Kristóf Nagy, Z., 2022. Raman-based real-time dissolution prediction using a deterministic permeation model. Int. J. Pharm. 617. https://doi.org/10.1016/j.ijpharm.2022.121624.

Ibrić, S., Djuriš, J., Parojčić, J., Djurić, Z., 2012. Artificial neural networks in evaluation and optimization of modified release solid dosage forms. Pharmaceutics 4, 531–550. https://doi.org/10.3390/pharmaceutics4040531.

Kale, K., Hapgood, K., Stewart, P., 2009. Drug agglomeration and dissolution – what is the influence of powder mixing? Eur. J. Pharm. Biopharm. 72, 156–164. https://doi.org/10.1016/j.ejpb.2008.12.015.

Kalný, M., Grof, Z., Štěpánek, F., 2021. Microstructure based simulation of the disintegration and dissolution of immediate release pharmaceutical tablets. Powder Technol. 377, 257–268. https://doi.org/10.1016/j.powtec.2020.08.093.

Karimi-Jafari, M., Soto, R., Albadarin, A.B., Croker, D., Walker, G., 2021. In-line Raman spectroscopy and chemometrics for monitoring cocrystallisation using hot melt extrusion. Int. J. Pharm. 601, 120555. https://doi.org/10.1016/j.ijpharm.2021.120555.

Klukkert, M., Wu, J.X., Rantanen, J., Carstensen, J.M., Rades, T., Leopold, C.S., 2016. Multispectral UV imaging for fast and non-destructive quality control of chemical and physical tablet attributes. Eur. J. Pharm. Sci. 90, 85–95. https://doi.org/10.1016/j.ejps.2015.12.004.

Lee, W.B., Widjaja, E., Heng, P.W.S., Chan, L.W., 2021. Effect of excipient particle size distribution variability on compact tensile strength; and its in-line prediction by force-displacement and force-time profiling. Eur. J. Pharm. Sci. 159, 105703. https://doi.org/10.1016/j.ejps.2021.105703.

Li, W., Wang, L., Wang, X., Fang, G., Zhang, Q., Qiu, P., Tu, P., 2023. Prediction of dissolution profiles of sinomenine hydrochloride sustained-release tablets part I: using near-infrared spectra as predictors. New J. Chem. 47, 15291–15301. https://doi.org/10.1039/D3NJ01896B.

Loh, Z.H., Samanta, A.K., Sia Heng, P.W., 2015. Overview of milling techniques for improving the solubility of poorly water-soluble drugs. Asian J. Pharm. Sci. 10, 255–274. https://doi.org/10.1016/j.ajps.2014.12.006.

Lourenço, A.S., Schuster, T., Lopes, J.A., Kirsch, A., 2025. A non-linear modelling approach to predict the dissolution profile of extended-release tablets. Eur. J. Pharm. Sci. 204, 106976. https://doi.org/10.1016/j.ejps.2024.106976.

Maderuelo, C., Zarzuelo, A., Lanao, J.M., 2011. Critical factors in the release of drugs from sustained release hydrophilic matrices. J. Control. Release 154, 2–19. https://doi.org/10.1016/j.jconrel.2011.04.002.

Madzarevic, M., Medarevic, D., Vulovic, A., Sustersic, T., Djuris, J., Filipovic, N., Ibric, S., 2019. Optimization and prediction of ibuprofen release from 3D DLP printlets using artificial neural networks. Pharmaceutics 11, 544. https://doi.org/10.3390/pharmaceutics11100544.

Markl, D., Maclean, N., Mann, J., Williams, H., Abbott, A., Mead, H., Khadra, I., 2021. Tablet disintegration performance: effect of compression pressure and storage conditions on surface liquid absorption and swelling kinetics. Int. J. Pharm. 601, 120382. https://doi.org/10.1016/j.ijpharm.2021.120382.

Matsunami, K., Ryckaert, A., Vanhoorne, V., Kumar, A., 2025. Mathematical models of dissolution testing: challenges and opportunities toward real-time release testing. Int. J. Pharm. 669, 125002. https://doi.org/10.1016/j.ijpharm.2024.125002.

Mészáros, L.A., Madarász, L., Ficzere, M., Bicsár, R., Farkas, A., Nagy, Z.K., 2024a. UV/VIS-imaging of white caffeine tablets for prediction of CQAs: API content, crushing strength, friability, disintegration time and dissolution profile. Int. J. Pharm. 663, 124565. https://doi.org/10.1016/j.ijpharm.2024.124565.

Mészáros, L.A., Madarász, L., Kádár, S., Ficzere, M., Farkas, A., Kristóf Nagy, Z., 2024b. Machine vision-based non-destructive dissolution prediction of meloxicam-containing tablets. Int. J. Pharm. 655, 124013. https://doi.org/10.1016/j.ijpharm.2024.124013.

Muselík, J., Komersová, A., Kubová, K., Matzick, K., Skalická, B., 2021. A critical overview of FDA and EMA statistical methods to compare in vitro drug dissolution profiles of pharmaceutical products. Pharmaceutics 13. https://doi.org/10.3390/pharmaceutics13101703.

Nagy, B., Petra, D., Galata, D.L., Démuth, B., Borbás, E., Marosi, G., Nagy, Z.K., Farkas, A., 2019. Application of artificial neural networks for Process Analytical Technology-based dissolution testing. Int. J. Pharm. 567. https://doi.org/10.1016/j.ijpharm.2019.118464.

Novikova, A., Carstensen, J.M., Rades, T., Leopold, P.D.C.S., 2016. Multispectral UV imaging for surface analysis of MUPS tablets with special focus on the pellet distribution. Int. J. Pharm. 515, 374–383. https://doi.org/10.1016/j.ijpharm.2016.09.087.

Novikova, A., Carstensen, J.M., Zeitler, J.A., Rades, T., Leopold, C.S., 2017. Multispectral UV imaging for determination of the tablet coating thickness. J. Pharm. Sci. 106, 1560–1569. https://doi.org/10.1016/j.xphs.2017.02.016.

Pawar, P., Wang, Y., Keyvan, G., Callegari, G., Cuitino, A., Muzzio, F., 2016. Enabling real time release testing by NIR prediction of dissolution of tablets made by continuous direct compression (CDC). Int. J. Pharm. 512, 96–107. https://doi.org/10.1016/j.ijpharm.2016.08.033.

Péterfi, O., Kovács, B., Casian, T., Tőkés, E.O., Kelemen, É.K., Zöldi, K., Nagy, Z.K., Nagy, B., 2025. Comparison of surrogate models in tablet dissolution prediction: addressing the limitations of F_2 and introducing sum of ranking differences for model evaluation. AAPS J. 27, 118. https://doi.org/10.1208/s12248-025-01100-2.

Péterfi, O., Nagy, Z.K., Sipos, E., Galata, D.L., 2023. Artificial intelligence-based prediction of in vitro dissolution profile of immediate release tablets with near-infrared and raman spectroscopy. Period. Polytech., Chem. Eng. 67, 18–30. https://doi.org/10.3311/PPch.20755.

Peters, J., Bartscher, K., Döscher, C., Taute, W., Höft, M., Knöchel, R., Breitkreutz, J., 2017. In-line moisture monitoring in fluidized bed granulation using a novel multi-resonance microwave sensor. Talanta 170, 369–376. https://doi.org/10.1016/j.talanta.2017.03.105.

Sacher, S., Fink, E., Alva, C., Alberto Afonso Urich, J., Doğan, A., Herndler, V., Koutsamanis, I., Kushwah, V., Peter, A., Salar-Behzadi, S., Wilfling, K., Stranzinger, S., Zettl, M., Feng, X., Korang-Yeboah, M., Wu, H., Khinast, J.G., 2024. Real-time prediction of dissolution profiles of coated oral dosage forms. Int. J. Pharm. 666, 124841. https://doi.org/10.1016/j.ijpharm.2024.124841.

Sørensen, D.H., Christensen, N.P.A., Skibsted, E., Rantanen, J., Rinnan, Å., 2022. In-line fluorescence spectroscopy for quantification of low amount of active pharmaceutical ingredient. J. Pharm. Sci. 111, 2406–2410. https://doi.org/10.1016/j.xphs.2022.06.008.

Wu, J.X., Rehder, S., van den Berg, F., Amigo, J.M., Carstensen, J.M., Rades, T., Leopold, C.S., Rantanen, J., 2014. Chemical imaging and solid state analysis at compact surfaces using UV imaging. Int. J. Pharm. 477, 527–535. https://doi.org/10.1016/j.ijpharm.2014.10.064.

Wu, S., Yang, Y., Wang, L., Jia, C., Guan, Z., Chen, H., Zhu, Y., Li, W., 2024. Prediction of drug dissolution from sustained-release pellet by a portable near-infrared spectrometer. J. Drug Deliv. Sci. Technol. 102, 106424. https://doi.org/10.1016/j.jddst.2024.106424.

Yekpe, K., Abatzoglou, N., Bataille, B., Gosselin, R., Sharkawi, T., Simard, J.S., Cournoyer, A., 2015. Predicting the dissolution behavior of pharmaceutical tablets with NIR chemical imaging. Int. J. Pharm. 486, 242–251. https://doi.org/10.1016/j.ijpharm.2015.03.060.

Zeng, Q., Gao, X., Wang, L., Fang, G., Qian, J., Liu, H., Li, Z., Li, W., 2023. Impact of Raman mapping area and intra-tablet homogeneity on the accuracy of sustained-release tablet dissolution prediction. Eur. J. Pharm. Biopharm. 190, 161–170. https://doi.org/10.1016/j.ejpb.2023.07.012.

Zeng, Q., Wang, L., Wu, S., Fang, G., Liu, H., Li, Z., Hu, Y., Li, W., 2022. Dissolution profiles prediction of sinomenine hydrochloride sustained-release tablets using Raman mapping technique. Int. J. Pharm. 620, 121743. https://doi.org/10.1016/j.ijpharm.2022.121743.

Zhao, Y., Li, W., Shi, Z., Drennen, J.K., Anderson, C.A., 2019. Prediction of dissolution profiles from process parameters, formulation, and spectroscopic measurements. J. Pharm. Sci. 108, 2119–2127. https://doi.org/10.1016/j.xphs.2019.01.023.

Zhong, L., Gao, L., Li, L., Nei, L., Wei, Y., Zhang, K., Zhang, H., Yin, W., Xu, D., Zang, H., 2022. Method development and validation of a near-infrared spectroscopic method for in-line API quantification during fluidized bed granulation. Spectrochim. Acta A Mol. Biomol. Spectrosc. 274, 121078. https://doi.org/10.1016/j.saa.2022.121078.